Article

Polarimetric Imaging vs. Conventional Imaging: Evaluation of Image Contrast in Fog

Maria Ballesta-Garcia *[ID], Sara Peña-Gutiérrez, Aina Val-Martí and Santiago Royo [ID]

Centre for Sensor, Instrumentation and Systems Development, Universitat Politècnica de Catalunya (CD6-UPC), Rambla Sant Nebridi 10, E08222 Terrassa, Spain; sara.pena.gutierrez@upc.edu (S.P.-G.); ainaval25@gmail.com (A.V.-M.); santiago.royo@upc.edu (S.R.)

* Correspondence: maria.ballesta.garcia@upc.edu

Abstract: We compare conventional intensity imaging against different modes of polarimetric imaging by evaluating the image contrast of images taken in a controlled foggy environment. A small-scale fog chamber has been designed and constructed to create the necessary controlled foggy environment. A division-of-focal-plane camera of linear polarization and a linearly polarized light source has been used for performing the experiments with polarized light. In order to evaluate the image contrast of the different imaging modes, the Michelson contrast of samples of different materials relative to their background has been calculated. The higher the image contrast, the easier it is to detect and segment the targets of interest that are surrounded by fog. It has been quantitatively demonstrated that polarimetric images present an improvement in contrast compared to conventional intensity images in the situations studied.

Keywords: turbid media; fog; polarimetry; memory effect; polarimetric imaging; image processing; contrast; detection

1. Introduction

When light propagates through turbid media, the direction of propagation is randomized faster than its initial state of polarization. As a consequence, light is attenuated before the initial polarimetric properties are lost. This effect is known as the polarization memory effect [1–3]. The prolonged maintenance of the polarimetric state causes, in given conditions, polarimetric images to show better image contrast than conventional (intensity or RGB) images [4–6]. With higher contrast, distinguishing and detecting objects in a scene of interest is easier. For this reason, images obtained by detecting polarimetric properties are a promising alternative for imaging in applications through turbid media [7]. Fields such as navigation, transport, or surveillance could take advantage of this phenomenon. For these applications, the detection and identification of targets through adverse weather conditions such as fog or smoke are essential. Conventional imaging is often limited and breaks down at low visibilities. Due to the aforementioned characteristics, polarimetric imaging is being explored as a possible solution to surpass this limit [8–12]. Following this approach, some authors have already presented methods that use polarimetric imaging to improve the classical methods for object detection and to increase the working range in adverse weather conditions, such as in [13–15].

Polarization can be described using different formalisms. Here, the Stokes vector $\vec{S}$ is used to characterize the polarization state of a light beam [16]. $\vec{S}$ is determined from the six irradiance measurements of the light beam showed in Table 1.

Table 1. Irradiance measurements I (W/m^2) taken with ideal polarizers in front of a radiometer.

Name	Measurements
I_H	Horizontal linear polarizer (0°)
I_V	Vertical linear polarizer (90°)
I_{45}	45° linear polarizer
I_{135}	135° linear polarizer
I_L	Left circular polarizer
I_R	Right circular polarizer

Using the measurements presented in Table 1, the Stokes vector is defined as:

$$\vec{S} = \begin{pmatrix} I_H + I_V \\ I_H - I_V \\ I_{45} - I_{135} \\ I_R - I_L \end{pmatrix} = \begin{pmatrix} S_0 \\ S_1 \\ S_2 \\ S_3 \end{pmatrix}, \tag{1}$$

where S_0, S_1, S_2, and S_3 are the Stokes vector elements. These elements are specified relative to a local x—y coordinate system defined in the plane perpendicular to the vector of light propagation.

The polarized portion of the beam represents a net polarization ellipse traced by the electric field vector as a function of time. This ellipse has an ellipticity (ε) and orientation of the major axis (η) (azimuth of the ellipse) measured counterclockwise from the x-axis such that:

$$\varepsilon = \frac{S_3}{S_0 + \sqrt{S_1^2 + S_2^2}}, \tag{2}$$

$$\eta = \frac{1}{2}\arctan\left(\frac{S_2}{S_1}\right). \tag{3}$$

From $\vec{S}$, characteristics of the light beam such as the total irradiance (I), the degree of polarization (DOP), and the degree of linear polarization (DOLP) can be directly derived as:

$$I = S_0, \tag{4}$$

$$DOP = \frac{\sqrt{S_1^2 + S_2^2 + S_3^2}}{S_0}, \tag{5}$$

$$DOLP = \frac{\sqrt{S_1^2 + S_2^2}}{S_0}. \tag{6}$$

In this article, we present a study of the contrast of different modes of imaging in fog, comparing images obtained utilizing the intensity and the polarization properties of light. Recently, due to the growing potential of polarimetry in applications through turbid media, several studies on the subject have been published. Researchers have presented experiments using different types of targets and backgrounds, involving scattering, absorption, and reflection targets. In the experiments, they evaluate the performance of different polarimetric modes. For these studies, optical properties of the media were chosen to be consistent with applications in biological imaging [17–19]. Outdoor testing in fog has also been done based on infrared illumination [20]. It has been shown that the contrast improvement depends on the polarimetric optical properties of the background and the target [17]. Aside from targets and backgrounds, another factor to consider is the polarimetric response of the media. When interacting with fog, incident light experiences a sequence of near-forward-scattering events before it contributes to the backscattered light. As a result, the backscattering due to fog is depolarized with a detectable component in the same initial polarization [2].

Our study is based on inspecting different types of common materials with different polarimetric properties and colors (paper, wood, plastic, and metal) immersed in a medium that reassembles actual fog. To perform these experiments, we have developed an experimental setup capable of producing, containing, and controlling a foggy medium with the desired characteristics. Its construction and characteristics are detailed in the next section.

2. Materials and Methods

2.1. Experimental Setup

2.1.1. Fog Chamber

The experiment was carried out by developing and constructing a small-scale fog chamber enabled to reproduce, characterize, and control the levels of fog transmittance. The schematics are presented in Figure 1a and a photograph of the system in Figure 1b.
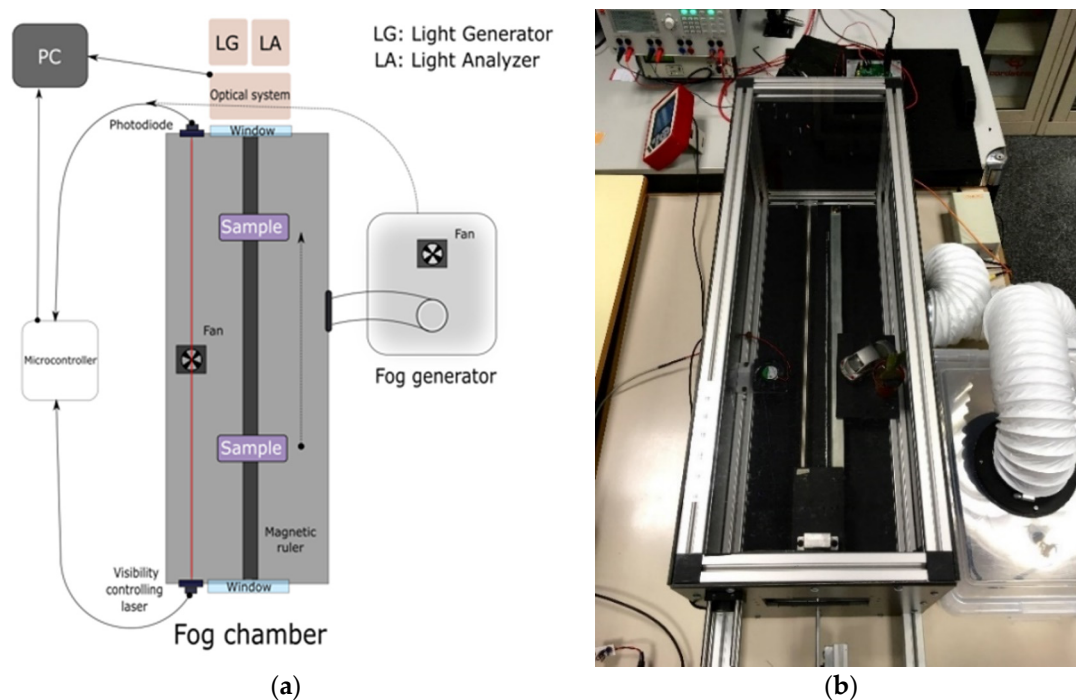

Figure 1. Small-scale fog chamber. Experimental setup used to perform the experiments: (**a**) Schematics; (**b**) Image of the fog chamber.

Despite that results in fog chambers are in general comparable to those expected in real fog, a real-life scenario has variabilities (dynamic fog, variety of droplet sizes, external illumination sources, etc.) that cannot be simulated in these set-ups. However, fog chambers give us a hint under controlled situations of what are the best alternatives to be tested in a real-world scenario.

Our fog chamber consisted of a 300 mm × 300 mm × 900 mm box with an aluminum structure covered by black methacrylate panels. One of the squared ends of the box had a hole in which the illumination and the detection optical systems were placed in the same geometrical plane. In the upper part of the chamber, an additional longitudinal optical path of 900 mm was enabled with a photodiode aligned to a collimated 635 nm laser source. These two elements were used to calibrate at all times the level of fog in the chamber through the experimentally measured optical transmittance (T):

$$T = I/I_0, \tag{7}$$

where I is the optical power measured at each moment, and I_0 is the initial optical power, when there is no fog in the box. Figure 2 shows the evolution of a typical cycle of dissipation of fog inside the box as a function of time.
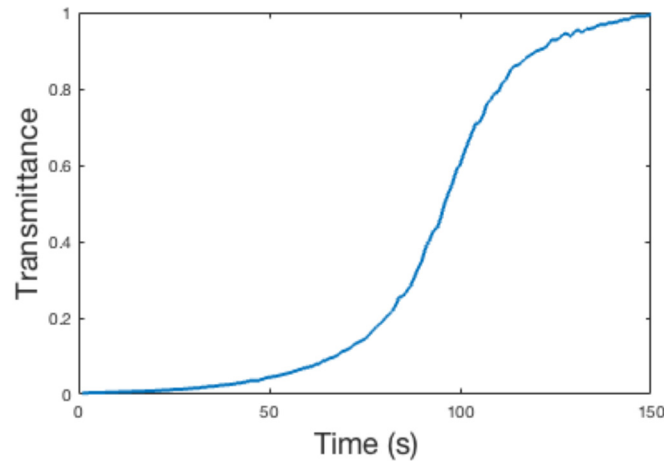

Figure 2. A cycle of fog dissipation inside the fog chamber.

To generate fog, a cold mist humidifier (Mist Maker DK5-24) was submerged in water in an external container. The humidifier was equipped with 5 powerful ultrasonic transducers that oscillate at a high frequency (1700 ± 40 KHz) to create water droplets. Due to the input energy generated by the transducers, the water surface is shattered into droplets that are forced to exit [21]. As a result, the dissipated water vapor accumulates and generates fog with droplets of a few microns in diameter [22]. Once the fog had been generated, it was injected into the fog chamber through a 10 cm diameter hole in its side using a fan. The procedure of fog generation was similar to the one described in [23]. Due to its characteristics, the fog entering the chamber tends to accumulate in layers at the bottom. An additional fan inside the box was used to distribute the accumulated fog uniformly. Once we arrived at the lowest desired transmittance T ~ 0 (around $T = 1 \times 10^{-4}$), the injection of fog was ceased. Dissipation of fog occurred naturally as the box is not airtight.

2.1.2. Illumination

To perform the experiments, a white light source model SCHOTT KL 1500 ELECTRONIC was used with a linear polarizer properly aligned. The polarization state of light was calibrated with a polarimeter model PAX1000VIS/M from THORLABS. The light was almost perfectly linearly polarized at $0°$ relative to the horizontal plane. The polarimetric characteristics of the light source (corresponding to the parameters defined in Equations (3)–(6) are presented in Table 2). The spectral characteristics of the light source are shown in Figure 3.

Table 2. Polarimetric characteristics of the illumination used for performing the experiments.

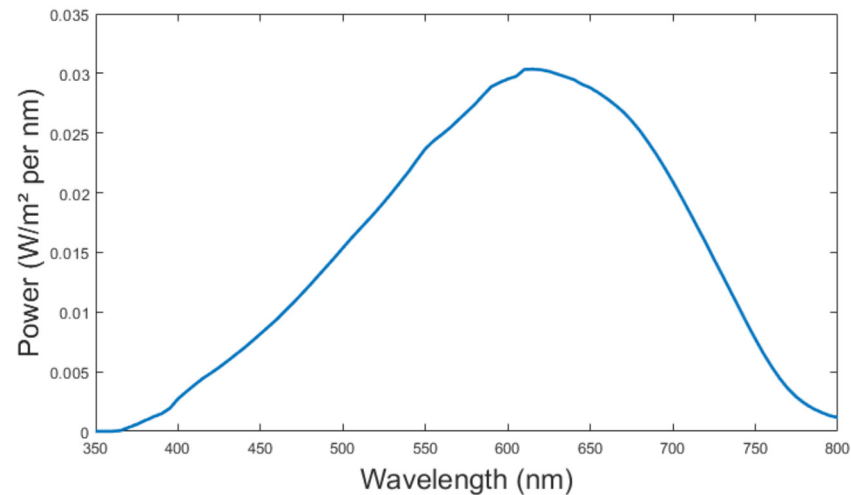| Parameter	Mean Value	Standard Deviation
Azimuth angle	-0.64 (°)	0.19
Ellipticity	-0.91 (°)	0.29
Degree of polarization	99.93 (%)	0.29
Degree of linear polarization	99.88 (%)	0.27

Figure 3. The spectral power distribution of the SCHOTT KL 1500 as a function of the wavelength.

2.1.3. Detection

The detector was a polarimetric camera PHX050S-PC from Lucid Vision Labs Phoenix, used in conjunction with a 25 mm Edmund Optics objective with the aperture set at f/1.4. This camera is a division-of-focal-plane (DoFP) imaging polarimeter of linear polarization. The sensor of this camera is based on micro-polarizer arrays. It has four linear polarizers ($0°$, $90°$, $45°$, and $135°$ aligned with respect to the horizontal position) grouped in one macro-pixel of 2×2 conventional pixels, i.e., each polarizer coincides with a pixel. A scheme of this configuration is shown in Figure 4. This configuration of the sensor allows the recovery of the linear polarimetric information of light and permits the obtainment of the first three Stokes parameters: S_0, S_1, and S_2 for each macro-pixel in the image.
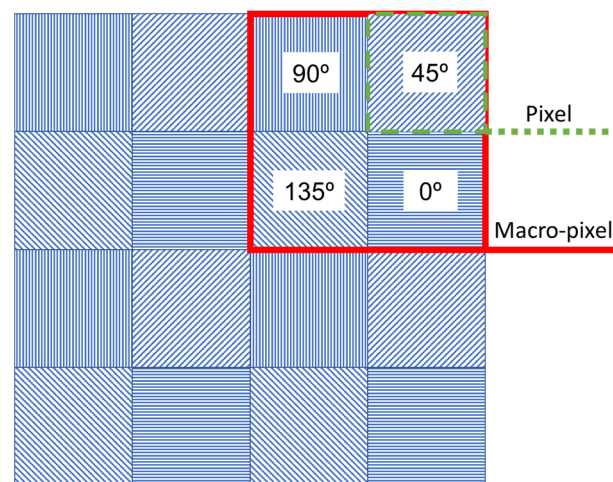

Figure 4. Scheme of the sensor of the polarimetric camera used as a detector. In front of each pixel, the corresponding polarizer is placed. The macro-pixel is the calculation unit.

2.1.4. Samples

The study aims to evaluate the behavior of some common materials. We used: a snippet of a standard white sheet of paper, a sample of grey expanded polystyrene (EPS) smoothed on the visible face, a metallic sample of a polished piece of aluminum, and a piece of pine plywood with the surface untreated.

To hold the samples of the different materials of study, a test plate organized in the form of a 2×2 matrix was used. The samples were placed on the test plate as shown in Figure 5. Each of the squared samples had a size of 30 mm $\times$ 30 mm, and the diameter of

the circular one was also 30 mm. The edge of the plate was covered with a black masking tape from THORLABS, and it was considered the background. The measured amount of visible light reflected from the tape was negligible (below 5%).
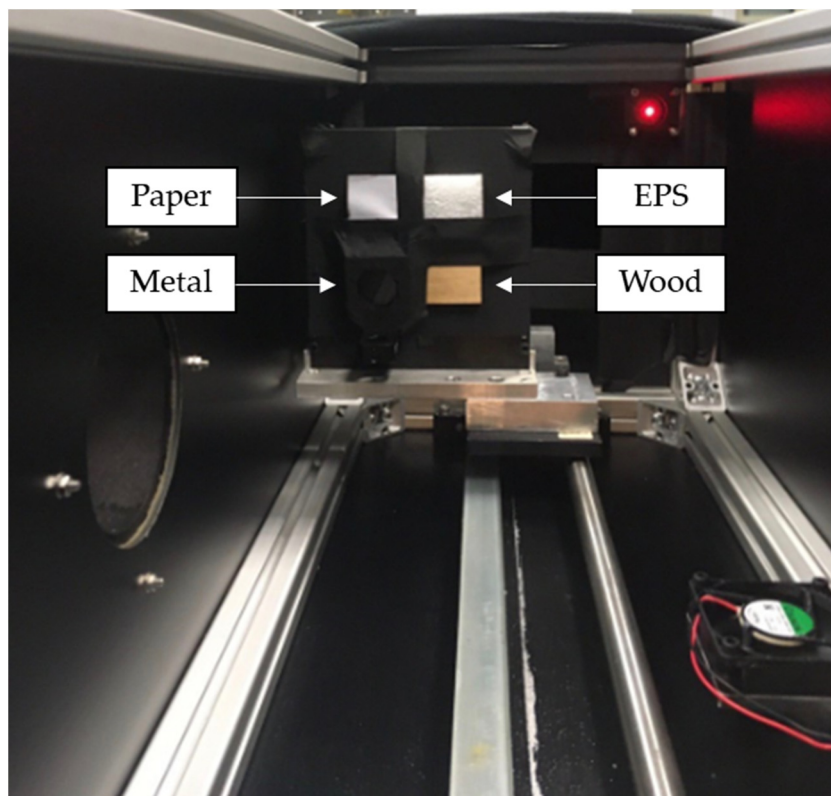

Figure 5. Test plate containing the targets of different materials inside the fog chamber. In the position top-left, there is a sample of a white sheet of paper; in top-right, a sample of gray expanded polystyrene (EPS); in bottom-left, a metallic object; and in bottom-right, a piece of wood.

The plate was placed inside the fog chamber. The light intensity at the edges and the center of the plate was verified, to ensure that the illumination was evenly distributed. To do this, the test plate was connected to a magnetic ruler built into the box. The ruler was allowed to move the plate longitudinally and explore the illumination properties at different distances. Intensity images of the setup without fog were taken. Grey levels were evaluated at different points of the images for different illumination configurations until all of the plate was evenly illuminated. The final configuration showed a deviation in an intensity below 2% between the edges and the center of the plate. For that configuration, the distance between the test plate and the illumination/detection plane was 650 mm. Then, the imager was properly refocused to obtain a clear image of the samples on the sensor at that distance.

Before the experiments, a polarimetric characterization of the behavior of each of the elements of the test plate was carried out. Each of the samples was illuminated with the same linear polarization state as the one described in Table 2 without fog. The polarimetric camera was used to obtain the linear Stokes polarimetric images of the scene. By combining the images of S_1, S_2, and S_3 according to Equation (5), the image of the degree of linear polarization (DOLP) was obtained. The DOLP exhibited by the reflected illumination of each material was evaluated from the acquired DOLP images. The results obtained are shown in Table 3. Paper, EPS, and wood were depolarizing materials with similar characteristics, and they behaved differently from metal and the background. As expected, dielectric materials did not maintain polarization, while metal and, in this case, the small amount of light reflected by the background (black masking tape) did.

Table 3. Degree of linear polarization of the reflected illumination for each of the elements of the test plate.

Material	DOLP
Paper	0.11
EPS	0.27
Metal	0.89
Wood	0.30
Background	0.75

2.2. Image Processing

2.2.1. Imaging Modes

The division of focal plane polarimetric cameras based on micro-polarizer arrays allow easy retrieval of images of the Stokes parameters [24]. As a result, in one shot, four images of the same scene corresponding to each of the polarization filters are obtained as raw images. With these data, the conventional intensity image can be calculated by simply adding two images with orthogonal polarizations. It is also possible to calculate the images corresponding to the linear Stokes parameters (S_1 and S_2), and other images based on usual parameters in polarimetry [17]. Table 4 shows all the image modes used in this study and also the acronym by which we will refer to them in the rest of this article. It is recalled that all those modes are simple linear combinations of the images obtained pixel by pixel or parameters usual in polarimetry. Our goal is now to compare the contrast obtained for each of these image modes through different fog transmittances.

Table 4. Imaging modes used in this study. From left to right: name, abbreviation used in this article, and means of obtaining them using the raw images (see Table 1).

Image Mode Name	Abbreviation	Computation
Intensity/Stokes 0	INT	$I_H + I_V = I_{45} + I_{135}$
Stokes 1	S_1	$I_H - I_V$
Stokes 2	S_2	$I_{45} - I_{135}$
Co-polarized	CO	I_H
Cross-polarized	CROSS	I_V
Degree of linear polarization	DOLP	$(S_1^2 + S_2^2)/\text{INT}$
Differential polarization	DIFF	$\text{CO} - \text{CROSS}$
Degree of co-polarization	POL	DIFF/INT

It should be noted that the concept of co-polarization corresponds to the detection of polarized light in the same state as the polarization of the emitted light. Instead, cross-polarization refers to the detection in the orthogonal state of that of the emission. In our case, the emission was at 0;, therefore, CO is the image obtained through the 0° polarizer (I_H) and CROSS the one corresponding to the 90° polarizer (I_V). Due to the configuration used, the differential polarization (DIFF) mode, which is defined for any general CO and CROSS component, is calculated by subtracting I_V from I_H in this study. Thus, in this particular experiment, the DIFF mode was equal to the Stokes 1 mode.

Figure 6 shows an example of the recovered images at different fog transmittances for the different image modes proposed in Table 4.
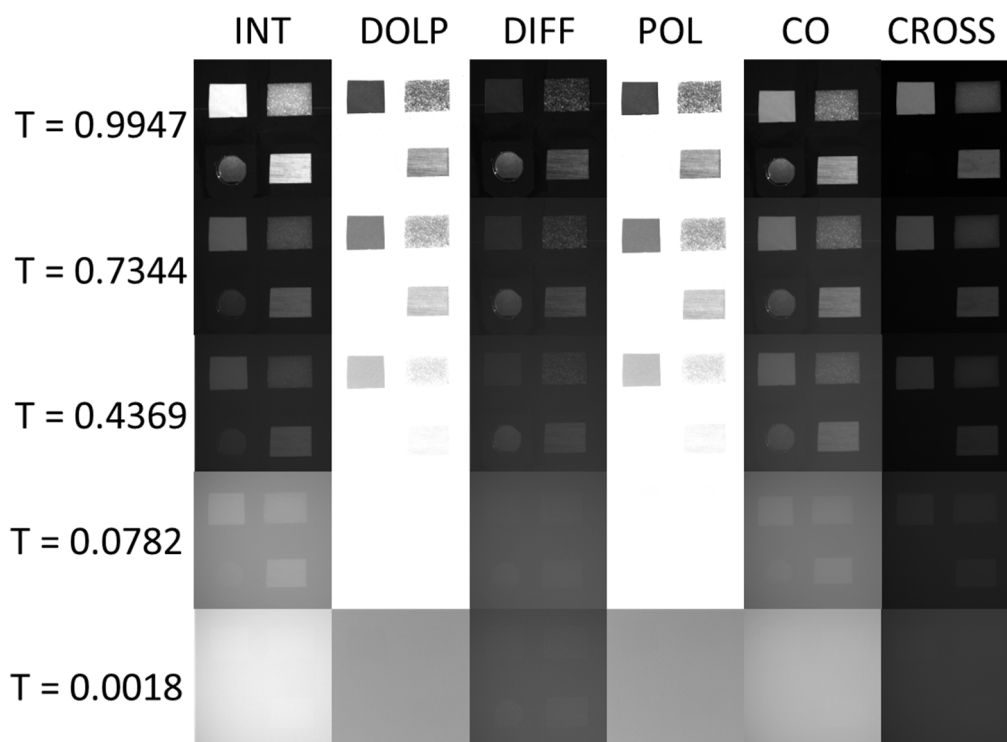
Figure 6. Images of the samples for the different image modes described in Table 4 under different fog transmittances, arranged in rows. T ~ 1 (**top**) corresponds to the absence of fog, while T ~ 0 (**bottom**) corresponds to the presence of very dense fog.

2.2.2. Michelson Contrast

When working in turbid media, and even more in a regime with very low transmittance, it is very difficult to quantify the degree of presence of an object visually. The point of this study is the quantification of the contrast to show the optimal imaging mode against materials and opacity of the medium. Even if it is not perceptible on the image, image processing performs better for those images with higher values of contrast.

Contrast is the difference in luminance that makes an object (or its representation in an image) distinguishable. In general, it is defined as the relative difference in intensity between two points in an image. It is usually used to quantify the ability to differentiate a sample from the background. In the literature, there exist numerous ways of calculating the contrast in an image [25]. In this study, we have used the Michelson contrast, as it is generally accepted as the most usual representation valid for all types of scenes when contrast is based on the most and the least intense points in the image irrespective of their surface area, frequency, or relative separation [26]. It is defined as:

$$C = \left| \frac{I_{obj} - I_{bg}}{I_{obj} + I_{bg}} \right|, \tag{8}$$

where I_{obj} is the average intensity of the sample of interest, and I_{bg} is the average intensity of a very specific zone corresponding to the test plate covered with the absorbent black masking tape.

To calculate the contrast, an area over a sample was selected on an image of reference with no fog. The selected area was adjusted in the central part of the sample, avoiding the boundaries. Once the area was defined, it was used for the same sample in all of the imaging modes for all the visibilities. This procedure was completed for each sample. The intensity of a sample was the average intensity over the area in the selection. The

intensity (I_{obj}) used to compute the contrast was the average over 10 images with the same transmittance.

3. Results

Figure 7 shows the evolution of the contrast between the selected sample and the background of the different image modes described in Table 4 for the four materials considered: (a) paper, (b) EPS, (c) metal, and (d) wood, measured at 45 different fog transmittance levels. The results obtained for the dielectric materials (paper, wood, and EPS) are comparable, while the metallic material behaves differently in coherence with what was observed in Table 3.
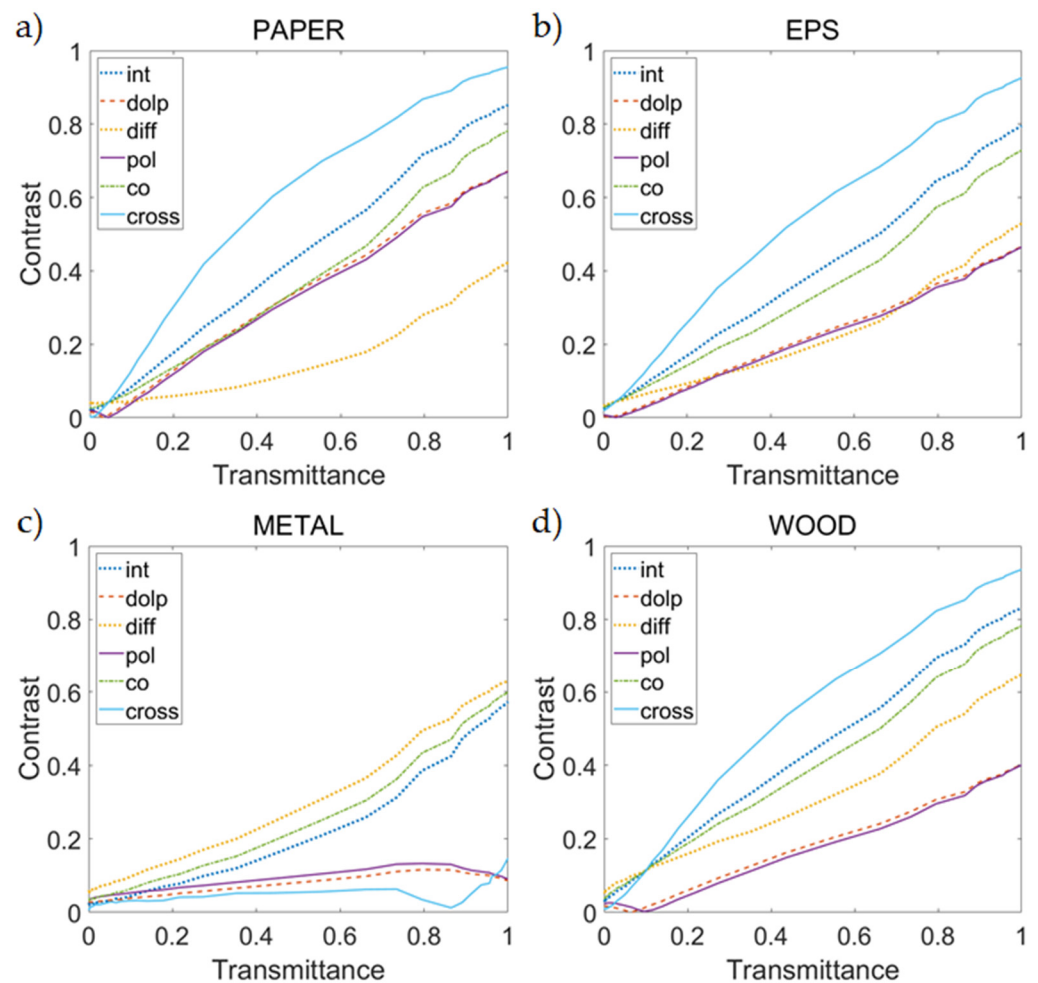
Figure 7. Michelson's contrast obtained for the image modes described in Table 4, at different transmittances. Each subfigure shows the result for different materials: (**a**) paper, (**b**) EPS, (**c**) metal, and (**d**) wood.

Figure 8 corresponds to the lowest transmittance range of Figure 6, from T ~ 0 to T = 0.1, which is related to very dense fog. This range has been expanded to observe the behavior better at the threshold of distinguishability for each of the materials: (a) paper, (b) EPS, (c) metal, and (d) wood. A horizontal black line has been drawn in all of the subfigures marking the contrast value 0.05 that will be useful in the discussion.
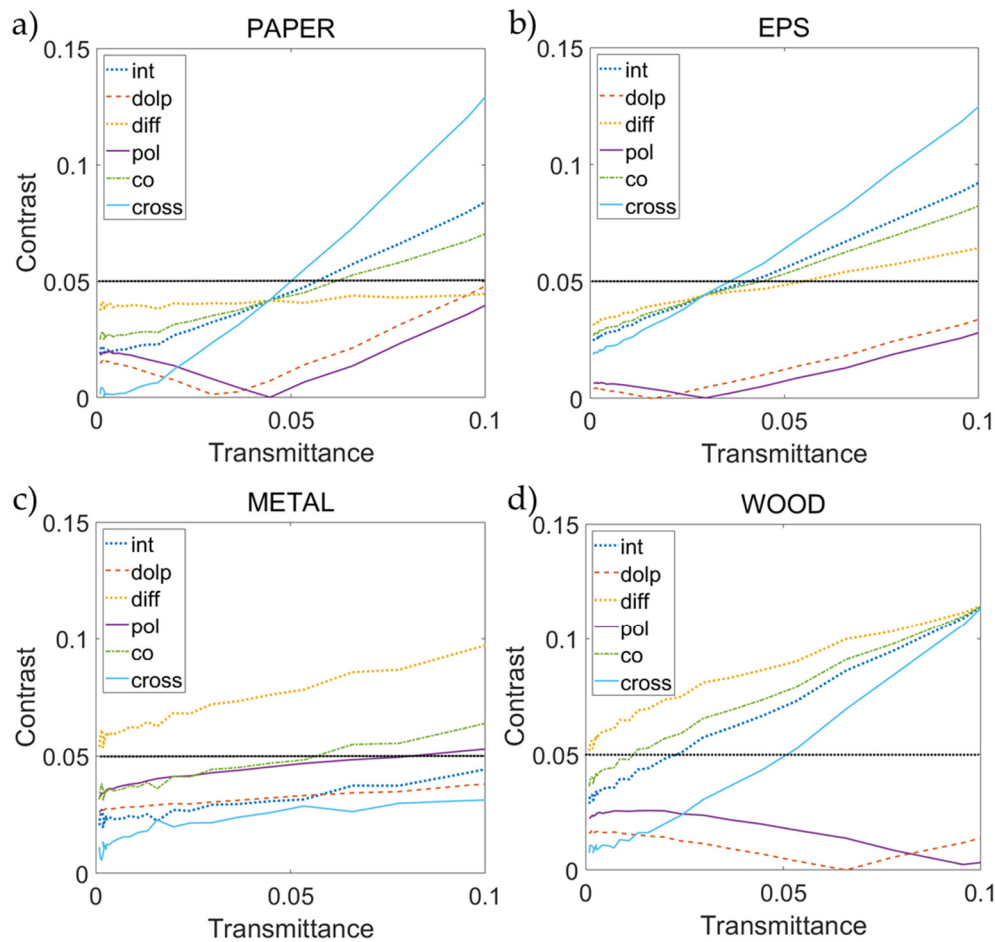
Figure 8. Michelson's contrast obtained for the image modes described in Table 4, at different transmittances. Each subfigure shows the result for different materials: (**a**) paper, (**b**) EPS, (**c**) metal, and (**d**) wood. Black line marks the 5% contrast threshold.

As a general trend, Figures 7 and 8 show that there is always a polarimetric image mode that presents a better contrast than the intensity image, even for higher transmittances. In the case of dielectrics, the mode with the higher contrast corresponds mostly to the CROSS image, while in the case of metal, the mode with the higher contrast is the DIFF image.

4. Discussion

To define a standard visibility value, a contrast threshold of 0.05 (5%) is settled as the distinguishable limit for the human eye [27]. For the analysis of the results obtained, we will use this convention. Therefore, a sample with a contrast below 5% will be considered as not detectable inside the fog.

The results presented in the previous section show the advantages that the use of polarimetric imaging can bring in the detection and the segmentation of objects embedded in turbid media. We proved that is possible to distinguish objects made with commonly encountered materials under the presence of fog using their polarimetric signature when conventional imaging fails. As it was mentioned in the introduction, this effect could have direct applications in fields related to transport in different media or surveillance in adverse weather conditions.

The contrast improvement is shown to be dependent upon the optical properties of the target and the turbid media. In general, backscattered light from targets exists primarily in the co-polarized component. For materials preserving polarization (such as metals), this effect is evident. In Figure 6 it can be seen that the metallic sample is not detectable at

all in the CROSS mode, whereas it is in the CO mode. In the case of dielectric materials, this effect is less pronounced because they mainly reflect depolarized light. As a result, co-polarized and cross-polarized components are almost evened out. In Figure 6 it can be seen how dielectric samples in the CO mode are only slightly brighter than in the CROSS mode. Finally, it is also possible to characterize the polarimetric properties of our fog using images in Figure 5. Comparing CO and CROSS mode images for T = 0.0018, it is proved that the generated fog is mainly backscattering light in the co-polarized component, as long as the grey level in the CO mode is higher than in the CROSS mode.

As a general tendency, Figure 7 shows that there is always a polarimetric image mode that presents a greater contrast than the intensity image, even for greater transmittances. In the case of dielectrics, the mode with the higher contrast corresponds to the CROSS image. Because fog reflects mainly in the co-polarized component of light, the CROSS mode can be used to filter out the blurring effect of fog, or at least to mitigate it. Considering that dielectric materials are mainly depolarizing, so they are returning co- and cross-polarized light, and the CROSS mode filters the fog effect without losing all the light returning from the sample. As a result, the image is cleaned of fog, and the sample is better defined. Due to it, the CROSS mode shows the greatest contrast. In comparison with dielectrics, metals reflect only on the co-polarized component of light. So, only imaging modes collecting the co-polarized component can detect metallic samples. From these modes, the DIFF image is the one presenting the highest contrast in our study, followed by the CO mode. The slight improvement of the DIFF mode in front of the CO mode comes from its capability to subtract the small traces of cross-polarized light coming from depolarization. For a metal embedded in fog, the DIFF mode gives a clear version of the CO mode. However, the absolute contrast will be always smaller than that from dielectrics, because the blurring effect of fog cannot be canceled using imaging modes that collect the co-polarized component.

For very low transmittances (from T = 1×10^{-4} to T ~ 0.05), which correspond to very dense fog, the contrast for the intensity mode is, in general, below the visibility threshold (5%), as it can be seen in Figure 8. Therefore, all the samples will not be distinguishable when using the intensity image. At this range of transmittance, the DIFF polarimetric mode shows the highest contrasts. The DIFF mode, based on subtracting the cross-polarized component from the co-polarized one, is one of the most popular techniques for increasing contrast using polarization in biomedical microscopy [28]. This study shows that the same improvements presented through biological tissue can be obtained in very dense fog.

For slightly higher transmittances (from T ~ 0.05 to T ~ 0.1), the DIFF mode continues to prevail for the metallic sample, but there is a change of behavior in the case of dielectric samples. At this range of transmittances, the fog-filtering effect of the CROSS mode can be applied because enough light arrives from the samples. As a result, there is a modification of the contrast tendencies, and the CROSS mode becomes dominant.

To sum up, by using the intensity image, it would not be possible to distinguish any of the samples through the fog at the lowest ranges of transmittance. However, DIFF and CO polarimetric modes show contrasts above distinguishability when intensity fails. In the case of metal and wood, the DIFF mode exceeds the threshold even for transmittances below 0.05. For paper and EPS, the CROSS mode is the first to surpass the threshold. With this study, we confirm that polarimetric imaging modes enable the detection of objects not distinguishable in the intensity image mode. In addition, for higher ranges of transmittance, polarimetric modes present higher contrasts than the intensity mode, proving that polarimetric imaging modes can help and have advantages in detecting materials through foggy media.

5. Conclusions

The Michelson contrast has been used to evaluate the contrast of images of different materials taken within a foggy medium using polarimetric imaging modes and conven-

tional intensity imaging. Using the latter, we assumed that a contrast below 5% does not allow us to distinguish the sample of interest.

For small transmittance, differential polarization (DIFF) imaging modes have shown contrasts above the threshold of distinguishability, while the intensity mode stays always below it. This higher contrast has the potential to enable the detection and segmentation of objects in turbid media with greatly reduced visibility. As a result, this study proves the usefulness of polarimetric imaging in turbid media, as it provides an interesting alternative to intensity images.

The different behavior between the studied materials has also been evaluated. In all cases and regardless of the type of material, we found that for very small transmittances, the mode with the highest contrast was the differential polarization image (DIFF). When the transmittance increases, for materials with dielectric characteristics (wood, paper, and expanded polystyrene), the image with the best contrast is that obtained using cross-polarization (CROSS), while metal maintains its initial behavior, with DIFF always being the mode with better performance.

Author Contributions: Conceptualization, M.B.-G., S.P.-G. and S.R.; methodology, M.B.-G. and S.P.-G.; software, A.V.-M.; validation, M.B.-G.; formal analysis, M.B.-G. and A.V.-M.; data curation, M.B.-G.; writing—original draft preparation, M.B.-G.; writing—review and editing, S.R.; supervision, S.R.; project administration, S.R.; All authors have read and agreed to the published version of the manuscript.

Conflicts of Interest: The authors declare no conflict of interest.

References

1. Xu, M.; Alfano, R.R. Random Walk of Polarized Light in Turbid Media. *Phys. Rev. Lett.* **2005**, *95*, 213901. [CrossRef] [PubMed]
2. MacKintosh, F.; Zhu, J.X.; Pine, D.J.; Weitz, D.A. Polarization memory of multiply scattered light. *Phys. Rev. B* **1989**, *40*, 9342–9345. [CrossRef]
3. Van Der Laan, J.D.; Wright, J.B.; Scrymgeour, D.A.; Kemme, S.A.; Dereniak, E.L. Evolution of circular and linear polarization in scattering environments. *Opt. Express* **2015**, *23*, 31874–31888. [CrossRef] [PubMed]
4. Lewis, G.D.; Jordan, D.L.; Roberts, P.J. Backscattering target detection in a turbid medium by polarization discrimination. *Appl. Opt.* **1999**, *38*, 3937–3944. [CrossRef]
5. Kartazayeva, S.A.; Ni, X.; Alfano, R.R. Backscattering target detection in a turbid medium by use of circularly and linearly polarized light. *Opt. Lett.* **2005**, *30*, 1168–1170. [CrossRef]
6. Walker, J.G.; Chang, P.C.Y.; Hopcraft, K.I. Visibility depth improvement in active polarization imaging in scattering media. *Appl. Opt.* **2000**, *39*, 4933–4941. [CrossRef]
7. Goudail, F.; Tyo, J.S. When is polarimetric imaging preferable to intensity imaging for target detection? *J. Opt. Soc. Am. A* **2010**, *28*, 46–53. [CrossRef] [PubMed]
8. Rozé, C.; Maheu, B.; Gréhan, G.; Menard, J. Evaluations of the sighting distance in a foggy atmosphere by monte carlo simulation. *Atmos. Environ.* **1994**, *28*, 769–775. [CrossRef]
9. Judd, K.M.; Thornton, M.P.; Richards, A.A. Automotive sensing: Assessing the impact of fog on LWIR, MWIR, SWIR, visible, and lidar performance. *Infrared Technol. Appl. XLV* **2019**, *11002*, 110021F. [CrossRef]
10. Schechner, Y.Y.; Narasimhan, S.G.; Nayar, S.K. Polarization-based vision through haze. *Appl. Opt.* **2003**, *42*, 511–525. [CrossRef] [PubMed]
11. Rowe, M.P.; Pugh, E.N.; Tyo, J.S.; Engheta, N. Polarization-difference imaging: A biologically inspired technique for observation through scattering media. *Opt. Lett.* **1995**, *20*, 608–610. [CrossRef]
12. Tremblay, G.; Roy, G. Study of polarization memory's impact on detection range in natural water fogs. *Appl. Opt.* **2020**, *59*, 1885–1895. [CrossRef]
13. Fade, J.; Panigrahi, S.; Carré, A.; Frein, L.; Hamel, C.; Bretenaker, F.; Ramachandran, H.; Alouini, M. Long-range polarimetric imaging through fog. *Appl. Opt.* **2014**, *53*, 3854–3865. [CrossRef] [PubMed]
14. Blin, R.; Ainouz, S.; Canu, S.; Meriaudeau, F. Road scenes analysis in adverse weather conditions by polarization-encoded images and adapted deep learning. In Proceedings of the 2019 IEEE Intelligent Transportation Systems Conference (ITSC), Auckland, New Zealand, 27–30 October 2019; pp. 27–32.

15. Blin, R.; Ainouz, S.; Canu, S.; Meriaudeau, F. A new multimodal RGB and polarimetric image dataset for road scenes analysis. In Proceedings of the 2020 IEEE/CVF Conference on Computer Vision and Pattern Recognition Workshops (CVPRW), Seattle, WA, USA, 14–19 June 2020; Volume 1, pp. 867–876.
16. Chipman, R.A. Polarimetry. In *Handbook of Optics*; Van Stryland, E.W., Williams, D.R., Wolfe, W.L., Eds.; McGraw-Hill: New York, NY, USA, 1995; Volume 2, pp. 22.1–22.37.
17. Nothdurft, R.E.; Yao, G. Effects of turbid media optical properties on object visibility in subsurface polarization imaging. *Appl. Opt.* **2006**, *45*, 5532–5541. [CrossRef] [PubMed]
18. Novikova, T.; Beniere, A.; Goudail, F.; De Martino, A. Contrast evaluation of the polarimetric images of different targets in turbid medium: Possible sources of systematic errors. *SPIE Def. Secur. Sens.* **2010**, *7672*, 76720Q. [CrossRef]
19. Nothdurft, R.; Yao, G. Expression of target optical properties in subsurface polarization-gated imaging. *Opt. Express* **2005**, *13*, 4185–4195. [CrossRef] [PubMed]
20. Vannier, N.; Goudail, F.; Plassart, C.; Boffety, M.; Feneyrou, P.; Leviandier, L.; Galland, F.; Bertaux, N. Comparison of different active polarimetric imaging modes for target detection in outdoor environment. *Appl. Opt.* **2016**, *55*, 2881–2891. [CrossRef]
21. Rodes, C.; Smith, T.; Crouse, R.; Ramachandran, G. Measurements of the Size Distribution of Aerosols Produced by Ultrasonic Humidification. *Aerosol Sci. Technol.* **1990**, *13*, 220–229. [CrossRef]
22. Kooij, S.; Astefanei, A.; Corthals, G.L.; Bonn, D. Size distributions of droplets produced by ultrasonic nebulizers. *Sci. Rep.* **2019**, *9*, 6128. [CrossRef]
23. Satat, G.; Tancik, M.; Raskar, R. Towards photography through realistic fog. In Proceedings of the 2018 IEEE International Conference on Computational Photography (ICCP), Pittsburgh, PA, USA, 4–6 May 2018; pp. 1–10.
24. Hickman, D.L.; Smith, M.I.; Kim, K.S.; Choi, H.-J. Polarimetric imaging: System architectures and trade-offs. In *Electro-Optical and Infrared Systems: Technology and Applications XV*; SPIE-Intl Soc Optical Eng: Bellingham, WA, USA, 2018; Volume 10795, p. 107950B.
25. Peli, E. Contrast in complex images. *J. Opt. Soc. Am. A* **1990**, *7*, 2032–2040. [CrossRef]
26. Bex, P.J.; Makous, W. Spatial frequency, phase, and the contrast of natural images. *J. Opt. Soc. Am. A* **2002**, *19*, 1096–1106. [CrossRef] [PubMed]
27. Dumont, E.; Cavallo, V. Extended Photometric Model of Fog Effects on Road Vision. *Transp. Res. Rec. J. Transp. Res. Board* **2004**, *1862*, 77–81. [CrossRef]
28. Kim, M.; Keller, D.; Bustamante, C. Differential polarization imaging. I. Theory. *Biophys. J.* **1987**, *52*, 911–927. [CrossRef]